Nuclear Inst. and Methods in Physics Research, A 976 (2020) 164275

Contents lists available at ScienceDirect

Nuclear Inst. and Methods in Physics Research, A

journal homepage: www.elsevier.com/locate/nima

AstrO: A portable cosmic ray telescope

S. Grazzi [a,b], L. Assandri [c], M. Battaglieri [b,d,a,*], C. Cardile [c], M. Corosu [b], F. Fontanelli [c,b], G. Ottonello [b], F. Parodi [b], L. Perasso [b,a], F. Pratolongo [b]

[a] Museo Storico della Fisica e Centro Studi e Ricerche Enrico Fermi, Roma, Italy
[b] Istituto Nazionale di Fisica Nucleare, Genova, Italy
[c] Università di Genova, Dipartimento di Fisica, Italy
[d] Thomas Jefferson National Accelerator Facility, Newport News VA, United States of America

ARTICLE INFO

Keywords:
Cosmic rays
Cosmic muons
SiPM
MPPC
Photon detector
Front-end electronics for detector readout
FPGA

ABSTRACT

This paper describes the design and performances of the AstrO (Astroparticle Outreach) cosmic muon telescope. The detector, contained in a trolley, is transportable and simple enough to be used by high-school students. The sophisticated data acquisition system is based on advanced DAQ technology and thanks to a simple interface is suitable for non-expert users. The detector is capable of measuring an integrated cosmic muon rate of 1–2 Hz with a precision (statistical and systematic) of a few percent in few hours of data taking. It can be used to detect variations induced by the solar activity, to determine the rate dependence on the geographical location (altitude and latitude) and to measure the cosmic muon rate attenuation due to surrounding high-density shielding such as rocks or concrete walls.

1. Introduction

The AstrO (Astroparticle Outreach) project started at the Istituto Nazionale di Fisica Nucleare in Genova (INFN Genova) few years ago as part of its Outreach activity to introduce Cosmic Ray and Particle Physics to high school students. Today it is part of the INFN project OCRA (Outreach Cosmic Rays Activities).

In conventional outreach programs, students attend formal lectures and perform measurements of secondary cosmic muon flux in laboratories of Universities or research Institutes. This approach has the advantage of making use of infrastructures available in professional labs but it is unfortunately not optimal considering the complications related to the logistic and the limited number of students that can be involved. We opted for an alternative approach building a dedicated, easy-to-use, portable – yet very accurate and sophisticated – detector. AstrO can be operated by students and teachers to measure the cosmic muon integral intensity variation at school location or outdoor (e.g. under caves or over hills), replicating historical experiments by mean of a modern technology.

The AstrO telescope measures the integral intensity of cosmic muons (integrated over the detector acceptance) with an accuracy of a few percent and the muon track angular distribution with a precision of 4 degrees in a few hours of data taking. With this accuracy it is possible to measure a tiny variation of cosmic muon intensity due to altitude, atmospheric pressure or variation induced by the solar activity (e.g. Forbush effect [1]).

The detector design and read out electronics have been the subject of two Master Theses of Genova University [2,3]. High school students, also involved in the Extreme Energy Events project (EEE) [4], contributed to the construction, the deployment and the operation of the telescope [5–7].

2. The detector

Portability, robustness and accuracy are the main characteristics of the AstrO cosmic muon telescope. The detector is made of eight plastic scintillator bars arranged in two parallel planes. Two long bars (60 x 8 x 2.5 cm^3) and two short ones (18 x 8 x 2.5 cm^3), placed perpendicularly below the long ones to form a grid, define two identical sets of hodoscopes. The detector layout is shown in Figs. 1 and 2. As can be seen, the long bars 7–8 (short 1–2) and 5–6 (3–4) define two pairs of detector with same geometrical acceptance, thus providing a redundancy that can be used to estimate the systematic error associated to the measurement of the cosmic muon integral intensity.[1] The custom electronics and a battery that provides the power for off-grid operations, are located at the bottom of the structure.

* Corresponding author at: Thomas Jefferson National Accelerator Facility, Newport News VA, United States of America.
E-mail address: battaglieri@ge.infn.it (M. Battaglieri).

[1] Other mixes of long and short bars combinations are also recorded by the DAQ but for simplicity we only report results for some of the pairs.
[2] Thanks to Wander Baldini, INFN — Ferrara (Italy).
[3] Kuraray Y-11 (200).
[4] 3M VM2000 reflecting coefficient R=0.985.

https://doi.org/10.1016/j.nima.2020.164275
Received 3 April 2020; Received in revised form 12 June 2020; Accepted 15 June 2020
Available online 17 June 2020

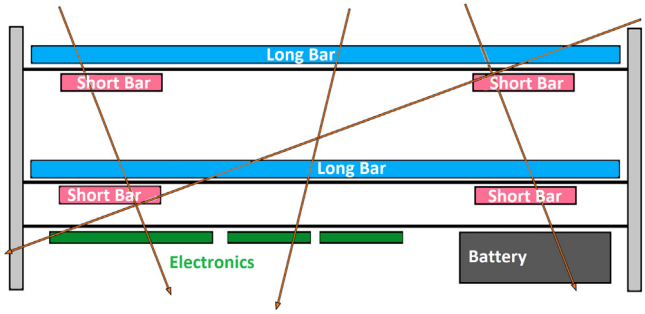

Fig. 1. Scheme of the AstrO detector with tracks of down-going cosmic muons.

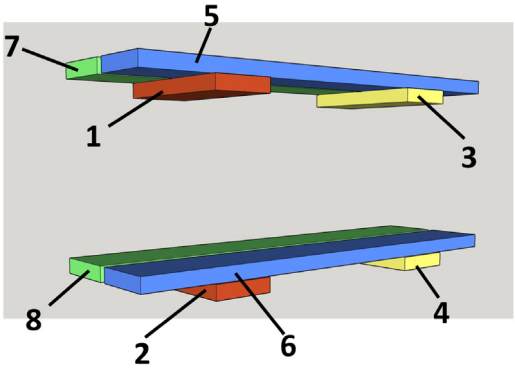

Fig. 2. AstrO Detector schematic geometry with scintillator tags.

The plastic scintillator bars[2] were extruded at FNAL-NICADD [8] with four holes (1.2 mm diameter) along the bar length. An efficient light collection is obtained by placing in each hole a 1.2 mm diameter Wave Length Shifter (WLS) fiber.[3] On one side of the bar, a highly reflecting foil[4] is used to reflect the light to a photo-sensor placed on the other side. The four fibers are collected together using a 3D printed plastic guide and coupled to a 3 × 3 mm^2 silicon photomultiplier (SiPM). An attenuation length of 60 cm guarantees a uniform light collection for any hit position along the bar. The bars were coated with TiO_2 to optimize the internal diffusion and increase the fraction of light captured by the WLS. Plastic bars were wrapped in 300 μm Gadolinium-deposited Mylar foils. The Gadolinium has one of the largest cross section for neutron capture (producing a cascade of gammas for a total energy of about 8 MeV) providing AstrO with an enhanced sensitivity to cosmic neutrons too. In this paper we report results obtained with a trigger that only selects cosmic muons. Detailed studies concerning AstrO neutron detection capability are in progress and results will be reported in a separate publication.

The SiPM signals are intensified by a trans-impedance amplifier and discriminated by an electronics custom circuit. The digital information is transferred to a Field Programmable Gate Array (FPGA) that performs the time coincidence between signals from different bars, manages the slow controls (SiPM bias voltages, thresholds, temperature) and writes data on a permanent memory. A detailed description of the front-end electronics and FPGA-based DAQ is provided in the next section. The detector is equipped with a 12 V battery,[5] capable of powering the system for about 12 hours. A custom circuit allows the user to switch between power grid and battery. The same circuit is automatically activated in case of power failure providing a solid backup.

The detector bars are held in place by an aluminum support. It is possible to vary both the distance between the two planes and the position of each pair of short bars in order to change the detector's geometrical acceptance. The nominal distance between the two planes is 22 cm. The same support holds the electronics boards and the battery. The AstrO detector, about 50 kg in weight, fits into a robust plastic trolley (76.5 x 48.5 x 30.5 cm^3) and it is easily transportable (see Fig. 4).

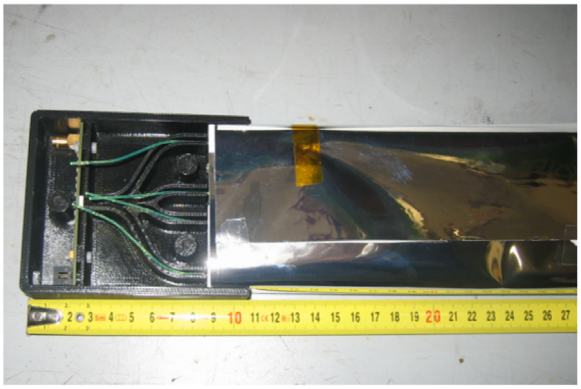

Fig. 3. Scintillator bar wrapped in Gd-deposited Mylar sheets: the four optical fibers transport the light to the SiPM.

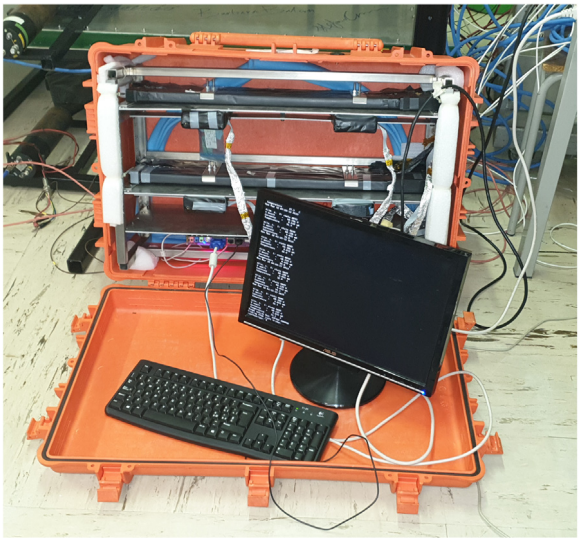

Fig. 4. AstrO detector inside the trolley.

3. Front-end electronics

AstrO photosensors are Silicon Photon Multipliers (SiPM),[6] with an active area of 3 × 3 mm^2 and a pixel pitch of 50 μm (3600 pixels in total). The SiPMs are operated approximately at 67 V with a dark count rate of 1000 kcps at 25 °C. The High Voltage (HV) bias network is derived by the one used to power the APDs in the Forward Tagger of the CLAS12 detector at Jefferson Lab [9]. The bias, adjustable for each SiPM with a precision of ≈ 1 mV, is generated as the difference between two sources: the cathode is biased via an HV module[7] [10] powering a block of four SiPMs which generates a voltage slightly higher than the highest voltage required; the voltage on the anode is fine-tuned subtracting a small voltage (up to ≈ 4 V) using a 12-bit Digital to Analog Converter (DAC). The reason for this elaborated circuitry is related to the fact that each SiPM needs a very precise voltage bias and, for cost reasons, we wanted to avoid using eight different power supplies.

[5] Pb battery RS PRO, 12 V, 7Ah.

[6] Hamamatsu S12572-050.

[7] Hamamatsu, model C11204-01.

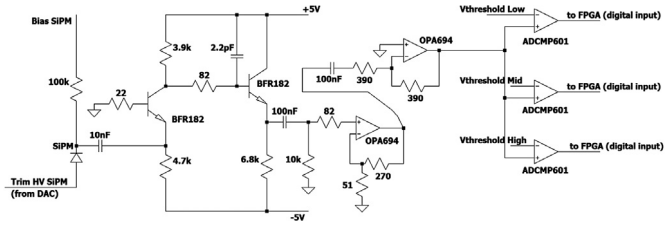

Fig. 5. Schematic of front-end electronics.

The HV system automatically tracks and corrects temperature changes thanks to a sensor[8] coupled to the HV module.

A front-end electronic board is shown in the top panel of Fig. 6, detailed schematic is shown in Fig. 5. It has been designed by the INFN-Genova Electronics Workshop with a three-fold purpose:

- to provide the bias voltage to each SiPM;
- to amplify the SiPM signal;
- to discriminate the amplified signal using three different thresholds set by voltage comparators.

The four layers printed circuit board (PCB) is 80 x 22 mm^2, 1.55 mm thick. The analog signal from each SiPM is capacitively coupled to a three stage custom-designed amplifier based on the CLAS-IC amplifier [9]. The first stage is based on a transistor[9] in a common base configuration, chosen for its low noise, high cut-off frequency and good stability. The input impedance of the amplifier (few tens of Ohms) is extremely low making it a trans-impedance amplifier with a gain equal to the collector resistance of the first transistor ($G_1 = 3.9$). A second transistor, in a common collector configuration, acts as a voltage-follower with a gain close to unity with the main function of decoupling the first from the second stage. The second stage is based on an operational amplifier[10] in a non-inverting configuration with high bandwidth, low power consumption and gain $G_2 = 6.3$. The third stage is built around another amplifier[11] in inverting configuration with $G_3 = -1$ that reverses the signal polarity, decouples the analog output and drives the discriminators. The analog output, coupled in AC, is routed to a LEMO connector for monitoring.

The overall current-to-voltage gain of the trans-impedance amplifier is given by the product of the single gain of each of the three stages: $G = G_1 * G_2 * G_3 = -24.6$. The output signal is then split into three parts and routed to three comparators.[12] Thresholds can be individually set by a four-channels DAC[13] used also to adjust the SiPM bias. The DAC is controlled by the FPGA board via I2C bus, as explained later. Comparators are impedance-matched to the cable bringing the discriminated signal to the FPGA by a 50 Ω series termination resistor at the output. Each SiPM is mounted on the back side of the PCB. To reduce the size of the amplifier, all passive components are in 0603 package, except the HV bias network components which are in 0805 package to improve insulation.

3.1. Control processor and counting electronics

The control processor and most of the digital electronics have been implemented on an FPGA[14] mounted on a development board.[15] The board and a full set of development tools accelerate and facilitate

[8] LM 94021.
[9] BFR182.
[10] OPA694.
[11] OPA694.
[12] ADCMP501.
[13] DAC7574.
[14] Altera/Intel Cyclone V.
[15] DE1-SOC board by Terasic [11].

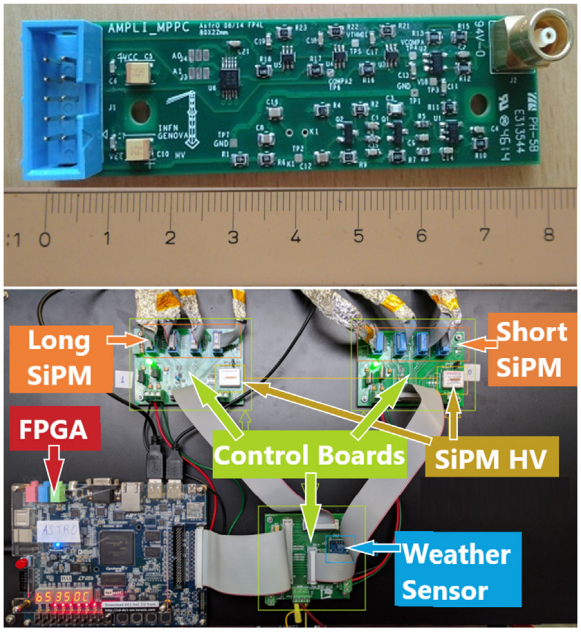

Fig. 6. Top: printed circuit board of the Front-end electronics. Bottom: view of all electronics boards.

the prototyping and development process. The board features a dual core processor,[16] 1 GB RAM, VGA monitor port, two multiplexed ADCs and one Gb-Ethernet port, keys and switches to input binary data (only for debugging purposes), seven-segment displays and two 40-pin connectors to interface the board with an external digital device (in our case used to connect the front-end electronics) plus many other devices, not used for this project, like g-sensor, etc.. The processor embedded inside the FPGA runs the Linux Operating System and, via the “bridge" built in the FPGA, configures the FPGA fabric and the I/O ports.

The FPGA firmware provides many features:

- a graphic display: this part is provided by the manufacturer and cannot be modified since the source code is not public;
- a basic display (used for debugging purpose): via switches and seven-segment displays it is possible to display immediately the content of each counter and most internal registers without the use of the processor;
- trigger logic, coincidences and counters: pulse coming from each SiPM is first asynchronously latched, synchronized to the system clock, digitally stretched and then sent to the combinatorial logic to count coincidences as described in the next section. To give the user maximum flexibility it is also possible to program up to four custom coincidences “on the fly” combining the outputs of the already existing coincidences, by writing the corresponding address into a dedicated register of the FPGA. Pulses from the logic are then counted by standard 32-bit counters which are reset and read by the processor using the bidirectional bridge implemented by the manufacturer between the hardware processor and the programmable logic in the FPGA;
- two I2C controllers to program the front-end chips, each controller managing four front-end boards. The code for the I2C controller has been extracted from the “opencores” site[17];
- two serial interfaces to set and monitor the SiPM biasing voltage via two dedicated power supplies.[18]

[16] 800-MHz ARM Cortex-A9.
[17] http://www.opencores.org/projects/i2c/, software written by Richard Herveille.
[18] Hamamatsu model C11204-01 [7].

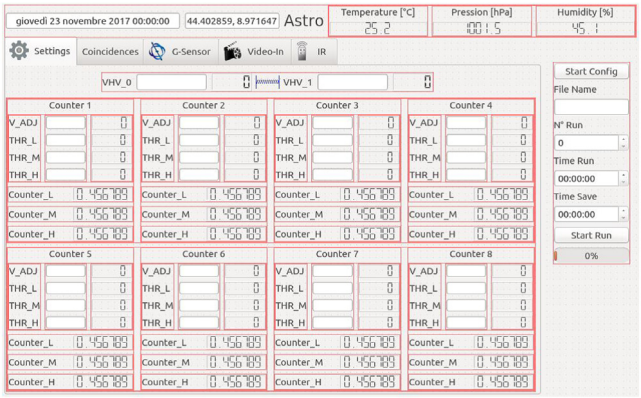

Fig. 7. View of the graphical interface created with Qt that allows to manage the detector without a PC. On the top right are shown the weather sensor values. The central window is divided into 8 squares, one for each scintillator bar. In these boxes, thresholds and voltages of each scintillator can be set and theirs instantaneous counts can be read.

3.2. Control software

As already mentioned, the development board contains a dual core processor running Linux OS. Graphic interface (VGA) and Ethernet connection simplifies the remote control of data acquisition and recording. All software (operating system, data acquisition program and auxiliary files) together with data files are written onto a 16 GB micro-SD card. A GPS receiver, connected to an USB port on the board provides a stable and reliable time-stamp recorded in the data stream. A dedicated sensor helps to monitor temperature, pressure and humidity.[19]

Two different versions of the control software were developed: a text interface (to be used for remote full-control and/or in batch mode), and a graphic interface (for local control by non-expert users; see Fig. 7). The control software reads the initial configuration set (voltages and thresholds, user defined coincidences, output file name, etc.) from a text file written on the micro-SD card and writes the output data in ASCII format onto the same device. The code is written in C/ C++ while the graphical user interface has been developed using Qt [13] libraries.

4. The trigger

The DAQ counts signals above a pre-defined threshold generated by:

- each individual bar (to test basic functionality and for calibration purposes);
- multiple combinations of two or more bars if the signals are in coincidence within a gate-time of 100 ns.

Referring to the bar numbering reported in Fig. 3, we implemented the following twelve combinations:

- short-short(SS): 1–2, 3–4;
- long-long(LL): 5–6, 7–8;
- long-short(LS): 1–5, 1–7, 2–6, 2–8, 3–5, 3–7, 4–6, 4–8;
- custom combinations.

The individual threshold values are optimized (see next section) to identify crossing Minimum Ionizing Particles — MIPs (cosmic muons). The possibility to use different thresholds will allow us to distinguish MIPs from gamma cascades generated by cosmic neutrons in the gadolinium layer, this possibility has non been exploited up to now, work is in progress. Thresholds are set, together with the selected trigger coincidences, via PC, using the software interface (see previous section).

[19] Bosch BME280 [12].

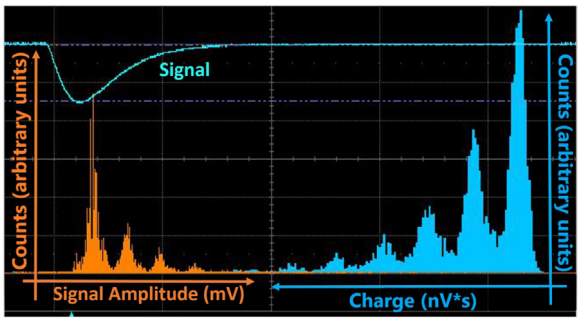

Fig. 8. Histograms showing the SiPM thermal noise signal: amplitude (orange) and charge (blue). Peaks generated by N and N + 1 pe are well separated. (For interpretation of the references to color in this figure legend, the reader is referred to the web version of this article.)

5. Detector calibration and commissioning

The threshold optimization and the assessment of the detection efficiency were performed during the detector commissioning in INFN Genova lab. A self-calibration procedure, to be applied before each run, was also defined and tested.

5.1. Single photo-electron calibration

As discussed in the previous section, the front-end logic compares the signal amplitudes to thresholds set at the beginning of the run. If the SiPM gain changes over time, the threshold may not be effective in cutting noise (if the gain increases) or may cut some good events associated to a low energy deposition (if the gain decreases). This is particularly critical for AstrO since no other information (charge, amplitude, signal shape) but counts over a fixed threshold are recorded. Since the amplitude of the SiPM signal (in mV) can be expressed as the product of the number of photo-electrons (pe) times the single pe amplitude (in mV), to avoid the dependence of rates on SiPM gain, it is possible to express the thresholds in pe and define a calibration procedure to measure the single-pe amplitude at the beginning of each run.

Fig. 8 shows an example of a SiPM signal and the charge/amplitude spectrum of thermal noise. Peaks correspond to one, two, and multiple-pe emission. Despite the Poissonian probability of thermal noise emission, the cross-talk generated in the silicon bulk increases significantly the chance to collect a higher number of pe, shifting to larger values the mean of the distribution. The self-calibration procedure uses the intrinsic SiPM thermal emission to measure the single-pe amplitude. The amplitude of the single-pe is measured for each SiPM in the following way: keeping the bias voltage constant, the threshold is first lowered in the range of the thermal noise (around 1–2 pe) then continuously increased in small steps of 1.2 mV collecting 2 s of data for each step. The sudden counting rate variation indicates that a transition between the emission of N and (N+1) pe happened. The distance (in mV) between peaks resulting by calculating the derivative of the counts function provides a good estimate of the single-pe amplitude.

The procedure is illustrated in Fig. 9: the top panel shows the rate resulting by changing the threshold, the bottom panel shows the derivative of the counts function. The two peaks correspond to N and (N+1) photoelectrons. At the beginning of each data taking, the self-calibration procedure scans the bias voltage of each SiPM and uses the measured single photoelectron amplitude to measure the SiPM gain and to convert the thresholds (stored in photoelectrons, see Table 1) to mV units.

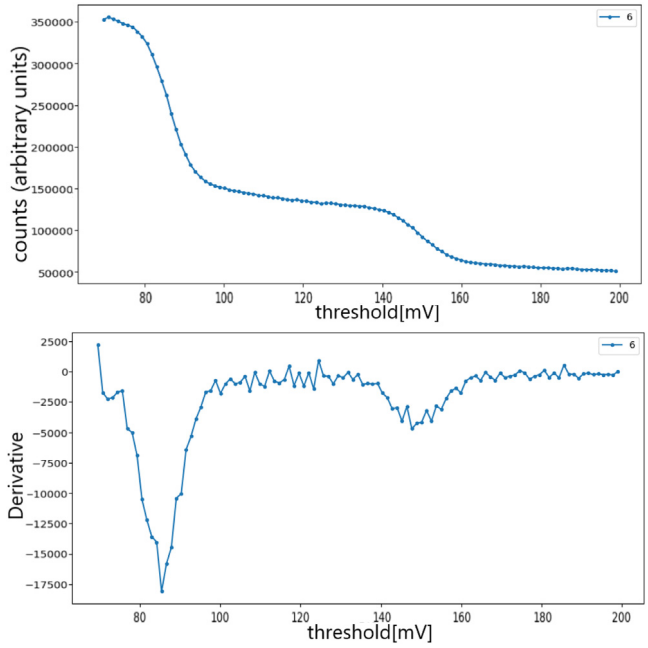

Fig. 9. Top: count measurement vs threshold. Bottom: derivative to find the two minimums corresponding to two consecutive photoelectrons.

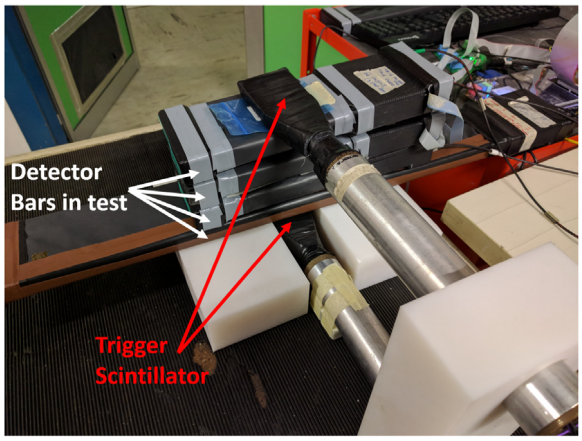

Fig. 10. The experimental set up used to characterize the scintillator bars. Red arrows point to trigger scintillators, while white arrows point to four specimen bars, all measured at the same time.

Table 1
SiPM signals: HV is the supply voltage for each SiPM; SiPM 2 has a different bias voltage because it has larger cells.

SiPM	HV (V)	Amplitude (mV)	Area (nV*s)
1	66.63	65	4.4
2	65.92	90	6.8
3	66.96	65	4.4
4	66.86	65	4.4
5	66.78	65	4.4
6	66.67	65	4.4
7	66.75	65	4.4
8	66.92	65	4.4

5.2. Threshold setting

To define the appropriate threshold value to separate physics events (crossing muons) from electronics noise, each scintillator bar was sandwiched between two detectors triggered by a cosmic muon trajectory.

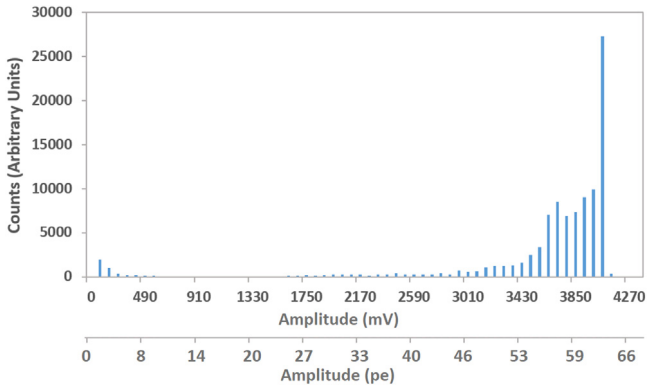

Fig. 11. Distribution of the signal amplitude for SiPM 6, expressed both in mV and in pe. Counts between 140 mV and 2400 mV correspond to cases where a cosmic muon triggers but the hit bar did not record the event (inefficiency). Amplitudes larger than 2400 mV correspond to cosmic muons.

The test setup is shown in Fig. 10. A digital oscilloscope[20] recorded amplitude and charge of a given bar. For each bar the cosmic muon energy spectrum, the absolute efficiency and the suitable MIP threshold value were measured and converted in pe units. With this setup we verified that attenuation length of light is negligible and this guarantees the same efficiency along bars. The typical signal amplitude distribution (in mV and pe) obtained in a calibration run is shown in Fig. 11. The number of events below threshold (2400 mV), normalized to the total counts, provides the inefficiency of a given bar. The small excess around 140–500 mV corresponds to the tail of the SiPM thermal noise while the peak around 3000–4100 mV corresponds to the MIP signal. Events accumulate on the right side of the histogram due to the saturation of the amplifier. A threshold of 1300–2600 mV (corresponding to ~20-40 pe) provides a clear separation between SiPM noise and MIPs. Table 2 shows thresholds (in mV and pe) and efficiency for each SiPM resulting from the calibration procedure.

5.3. Temperature dependence

The main factor affecting the SiPM gain stability is the sensor temperature. For a portable detector expected to operate in different environmental conditions (indoor, outdoor, warm and cold weather) the temperature variation can be sizeable (up to 30 °C) and an active temperature stabilization is practically impossible (or rather complicated to implement). For the SiPM used in AstrO, the $\frac{dG}{GdT}$ is about $2\%/°C$ [10]. The temperature dependence was mitigated by stabilizing the SiPM gain with a feedback loop locked on T. To control the Hamamatsu operating voltage the feedback loop uses the T measured in proximity of the electronics boards applying a linear correction with a coefficient of 65 $mV/^0C$.

Any further SiPM gain dependence on T or other parameters, is removed by splitting the total data acquisition time into several runs, no longer that one hour each, and applying at the beginning of each run the self-calibration procedure described above.

6. Monte Carlo simulations

The response of the AstrO detector to cosmic muons has been simulated using the GEMC simulation tool [14]. GEMC is an interface to GEANT4 libraries [15] that allows an easy description of the detector geometry, materials and active volumes as well as the environment where the detector is operated. Crossing cosmic muons are tracked in active materials recording the energy deposition and the time of

[20] (LeCroy WaveRunner 640Zi).

Table 2
SiPM thresholds (in mV and pe) and measured efficiency.

SiPM	Threshold (mV)	Npe	Efficiency (%)
1	2000	31	75
2	1800	20	90
3	2600	40	87
4	2600	40	85
5	1400	22	95
6	2400	37	92
7	1300	20	95
8	1600	25	85

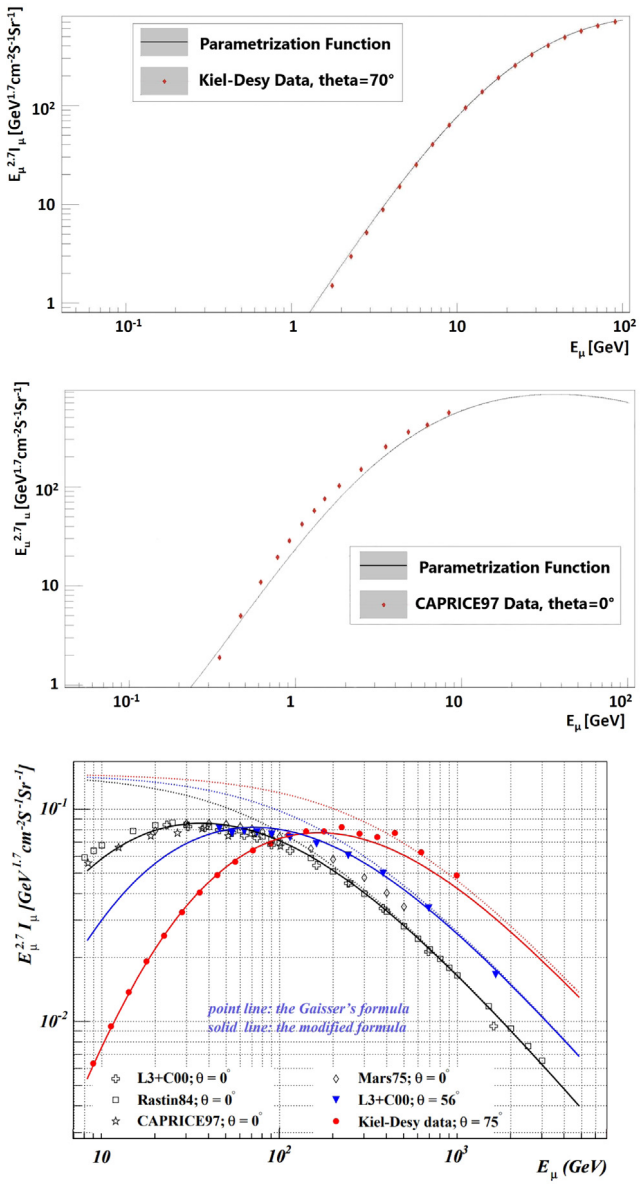

Fig. 12. Top: improved Gaisser parameterization for cosmic muon flux at two different thetas and including low energy muons are compared with available experimental data. Bottom: the cosmic muon flux compared to the existing measurements for higher energy.

the interaction. For each scintillator bar, light emission, collection (via WLS), and detection efficiency (see Table 2), as measured during calibration, were implemented in the code for a realistic description of the detector response to cosmic muon hits. Fig. 2 shows the AstrO geometry implementation in GEMC.

Table 3
Coincidences rates measured and results from simulation. The quoted errors are statistical only for simulation and a combination of statistical and systematic for data.

Bar comb.	Simulation rate (Hz)	Data rate (Hz)
Long-Long (LL)	2.1 ± 0.02	1.99 ± 0.02
Short-Short (SS)	0.46 ± 0.05	0.42 ± 0.01
Long-short (LS)	1.01 ± 0.05	1.02 ± 0.01

To simulate the cosmic rate measured by AstrO, the cosmic muon flux has been generated according to the parameterization reported in [16], an updated version of Gaisser's parameterization [17] of muon flux $dI_\mu(E_\mu, \theta_\mu)/dE_\mu$ that includes the curvature of Earth (all latitudes) and low energy muons ($E_\mu < 100$ GeV). The parameterization fits the measured data well in a wide range of energy and azimuthal muon angle θ_μ. Some comparisons are shown in Fig. 12.

Muons have been generated in the energy range E_μ 0.2–100 GeV over a semi-sphere surrounding the detector obtaining a uniform and flat distribution on a planar surface. The procedure is described in details in Ref. [18]. For energies lower than 0.2 GeV muons are absorbed by the atmosphere while the fraction of the spectrum for energies larger than 100 GeV is negligible. The overall normalization factor 1.06 muon/cm^2/min [19] has been used to obtain the absolute flux. For each event, simulations provide, per each scintillator bar, deposited energy and interaction time. In the off-line analysis coincidences between different combinations of scintillator pairs are counted in the same event, mimicking results obtained in the real measurement with AstrO FPGA-based data acquisition.[21] Simulations were performed considering a detector located at sea-level both outdoor, with no obstacles or surrounding material, and an in-door configuration which includes a detailed description of the Physics Department of Genova University. The combination in pairs of two of the 8 bars provides 28 geometrical coincidences. We focused on the combination of the two pairs of overlapping bars forming two LL, two SS and eight LS combinations. The simulated coincidence rates, as well as rates measured by AstrO in the in-door/outdoor configurations, are reported in Table 3. The good agreement between data and simulations demonstrate that the model used to generate cosmic muons and the GEANT4 description of the AstrO detector (inefficiency, geometrical acceptance, ...) are accurate at a level better than 10%.

7. Results

The AstrO telescope is designed to perform different kinds of measurements. It is capable of measuring the integral intensity of vertical muons (integrated over the detector acceptance) with the sensitivity of spotting variations due to solar activity (Forbush effect) or related to altitude or latitude change of the detector location; by comparing indoor to outdoor rates it provides the muon absorption factor due to the presence of surrounding materials; by changing the bars set-up it can measure the angular distribution of cosmic muons.

In this section we report the AstrO telescope precision and stability assessment, and the determination of the systematic error associated to the quoted rates.

7.1. Rate stability

As reported in the previous section, the good comparison of measured rates and simulation gave us confidence in a good understanding of the detector performance. The redundancy given by the identical geometrical acceptance of pairs of bars provides a solid cross check of systematic error on measured rates and doubles the statistics of each

[21] As described before, the analog signal corresponding to a muon crossing the detector is available as monitoring output of amplifiers but it is not recorded by the FPGA.

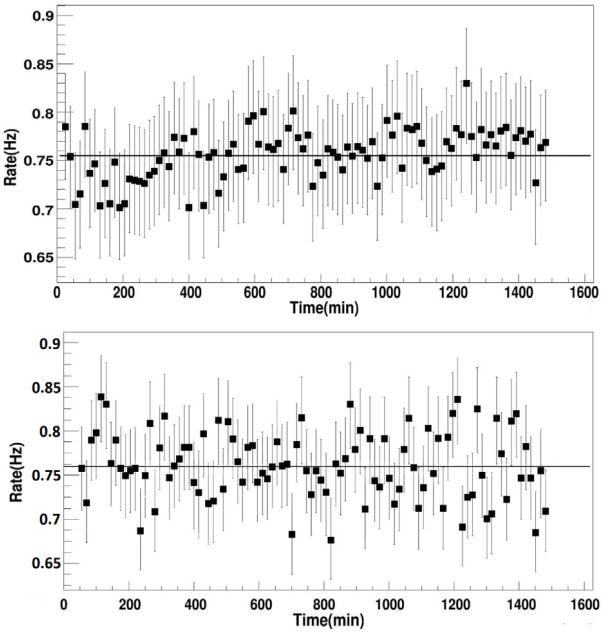

Fig. 13. Time distribution of LS counts for 1–5 (top) and 4–8 (bottom) bar pairs. Data show the stability of the system over an approximately 24 h interval. Errors are statistical only. The two mean values (indicated on the two graphs with a black line) are compatible within 1%.

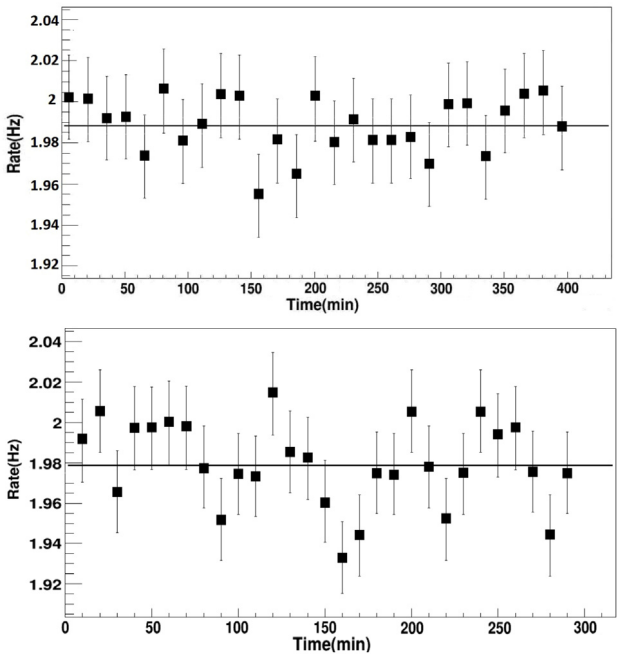

Fig. 14. Outdoor LL count rates. The top panel shows the reference measurement. The bottom panel shows the same measurement performed after four months and moving the telescope in different locations.

Table 4
Comparison between indoor (In) and outdoor (Out) AstrO rates measured in November 2018 (Run1) and February 2019 (Run2). The quoted errors are a combination of statistical and systematic uncertainties.

Position	Rate SS (Hz)	Rate LL (Hz)	Rate LS (Hz)
Run1-Out	0.42 ± 0.01	1.99 ± 0.02	1.02 ± 0.01
Run1-In	0.31 ± 0.01	1.46 ± 0.02	0.76 ± 0.01
Run2-Out	0.41 ± 0.01	1.98 ± 0.02	1.02 ± 0.01
Run2-In	0.30 ± 0.01	1.44 ± 0.02	0.74 ± 0.01

bar combination when combined together. We verified that over a short period of time (~day), similar pair rates agree within 1% (well below the statistical error). Fig. 13 shows the rates of two LS pairs (1–5 and 4–8) measured over 24 h.

To verify the stability of the detector and the reproducibility of the measurement over a longer period of time, we compared rates measured in a distance of several months and moving the detector to different locations.[22] Fig. 14 and Table 4 show the comparison of two data samples collected in November 2018 (Run1) and February 2019 (Run2) in Genova after a stress-test.[23] By comparing the average rates we estimated that the systematic error on the integral vertical muon intensity measured by AstrO is less than 3%.[24]

7.2. Rates comparison

For an absolute comparison of rates measured by AstrO we used as a reference the Oulu Cosmic Ray Station [20] that quotes an error on cosmic neutron rate < 1%. Fig. 15 shows the comparison between the cosmic muon absolute rate measured by AstrO in an 18-day-long run and the cosmic neutron rate variation reported by Oulu Station in the same period. The good agreement of the two measurements (well within the quoted error) prove the good quality of our data and the stability of measured rates.

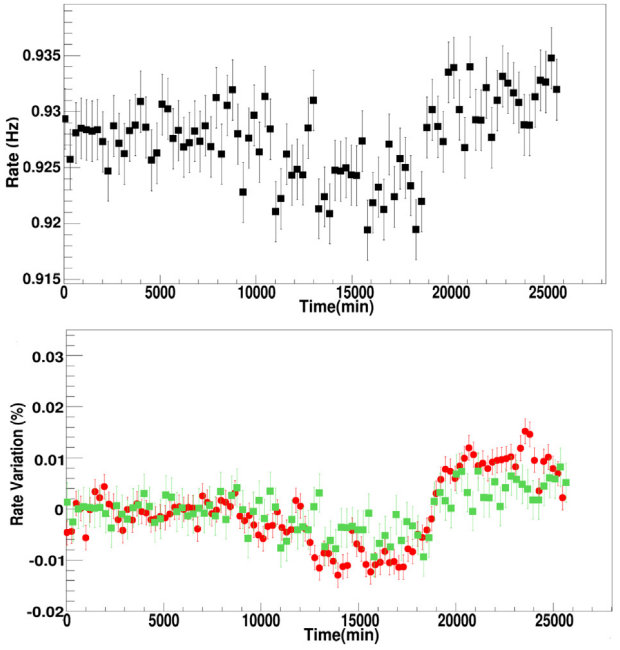

Fig. 15. The upper panel shows AstrO LL absolute cosmic muon rate measured between November 22 and December 10 2019. The bottom panel shows the rate variation in the same period of time (green) superimposed to Oulu measurement (red). (For interpretation of the references to color in this figure legend, the reader is referred to the web version of this article.)

[22] All rates are corrected to take in account atmospheric pressure variation. The procedure is similar to the one described in Ref. [20].

[23] Measurements were repeated after traveling AstrO by boat and car in different locations around Italy.

[24] Using as a reference the Oulu Neutron Monitor [20], we verified that the secondary cosmic flux did not vary significantly between the two periods of time when the measurements were performed.

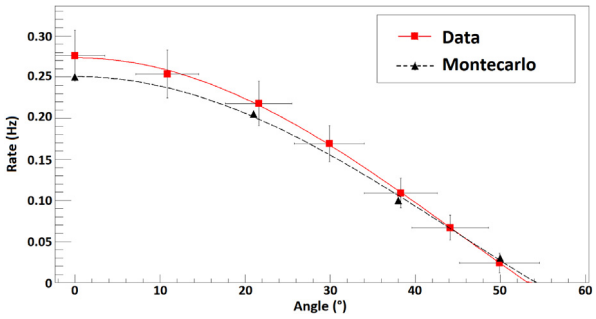

Fig. 16. Angular acceptance dependence of cosmic muons integral intensity as measured by AstrO (red), compared to MC simulations (black). MC and data does not include systematic error. (For interpretation of the references to color in this figure legend, the reader is referred to the web version of this article.)

Table 5
Sum of LS rates for four different latitudes.

Position	Latitude	Rate (Hz)
Genova Pre-Tour	44° 25' N	8.2 ± 0.2
Cagliari	39° 13' N	8.2 ± 0.2
Ratio GE-CA		0.99 ± 0.03
Oristano	39° 54' N	8.1 ± 0.2
Ratio GE-OR		1.00 ± 0.03
Porto Torres	40° 49' N	8.3 ± 0.2
Ratio GE-PT		0.98 ± 0.03
Genova Post-Tour	44° 25' N	8.1 ± 0.2

7.3. Cosmic muon angular distribution

As described in the previous section, the short scintillator bars can slip and change position, defining different angular acceptance for the SS combination. Cosmic muon trajectories can be selected between 0° to 50° with respect to the vertical direction. Fig. 16 shows the results of the measurement compared to the simulation as described in the previous section. The good agreement demonstrates that AstrO telescope is able to measure the dependence of the cosmic integral intensity as a function of the azimuthal angle with an accuracy of 4°.

7.4. Rate dependence on the location

In addition to the excellent performance shown above, the portability of AstrO detector allows one to measure the integral intensity of cosmic muons at different locations. Here we report the results of a measurement campaign in different cities in Italy (from Cagliari to Genova) with a variation of approximately 5° in latitude. Fig. 17 shows rates as a function of time as measured in three locations. The latitude and the corresponding measured rates are reported in Table 5. As expected by previous measurements [21], no significant variation was observed. Measurements of rates at different altitude and at different depth in a coal cave are currently underway and will be the subject of a separate report.

7.5. Cosmic muon absorption

The AstrO telescope is also able to measure the attenuation of the cosmic muon integrated intensity due to surrounding material. Besides outreach purposes, this feature is particularly useful to determine the experimental conditions of unmovable detectors shielded by building roofs or host in caves dug in rocks. For example this is true for the cosmic muon telescope network of the Extreme Energy Events (EEE) project [4]. In fact, EEE detectors are largely installed in schools or laboratories where a precise determination of surrounding materials is difficult and an effective way to compensate for different experimental conditions is highly valuable to normalize counts obtained by

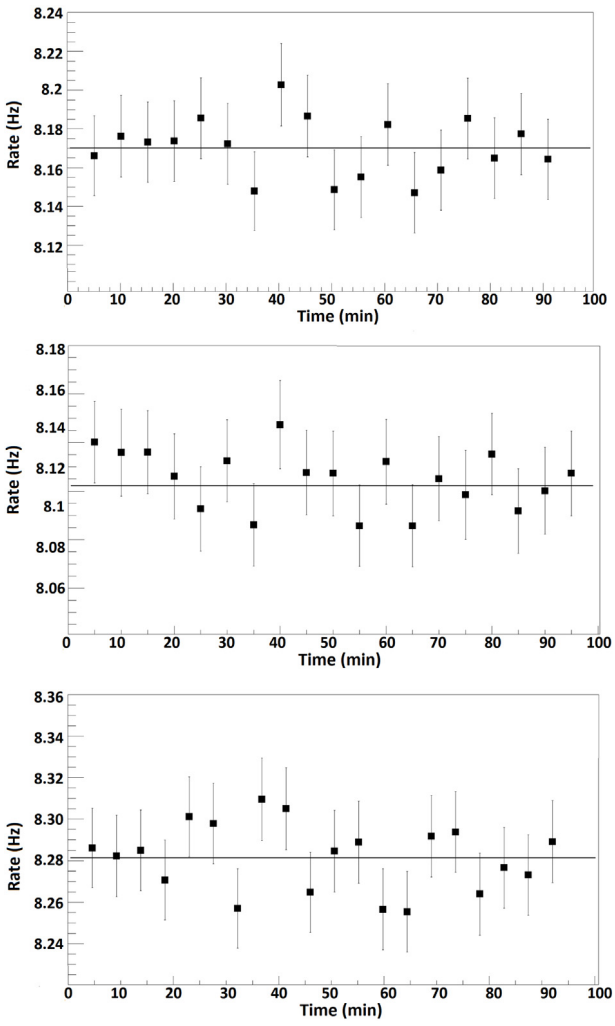

Fig. 17. Sum of LS rates measured in Cagliari (top) Oristano (middle) and P.Torres (bottom).

Table 6
Rates of all LS coincidences performed at Genova both Outside and inside Physics Department, and absorption ratio.

Position	Rate (Hz)	MC rate (Hz)
Outdoor	8.1 ± 0.2	8.1 ± 0.2
Indoor	6.0 ± 0.2	5.8 ± 0.2
Ratio	74% ± 4%	71% ± 4%

telescopes in different locations. Thanks to AstrO's mobility, a direct comparison of rates measured inside and outside the building provides an accurate determination of the effective absorption of the cosmic muons. As an example, Fig. 18 shows rates as measured inside the Department of Physics of Genova University (one of the EEE telescope location) compared to the measurement performed outdoor. Rates are compared to simulation results that include a detailed description of geometry and material of roof and walls of the building. Rates (indoor and outdoor) and the absorption factor (defined as the ratio of the two rates) are reported in Table 6.

8. Conclusion

The AstrO detector is a portable cosmic muon telescope designed and assembled as part of the outreach program of INFN Genova Unit. Making use of modern technology (plastic scintillator, SiPMs and FPGA-based DAQ) it is a transportable and easy-to-use detector that can be

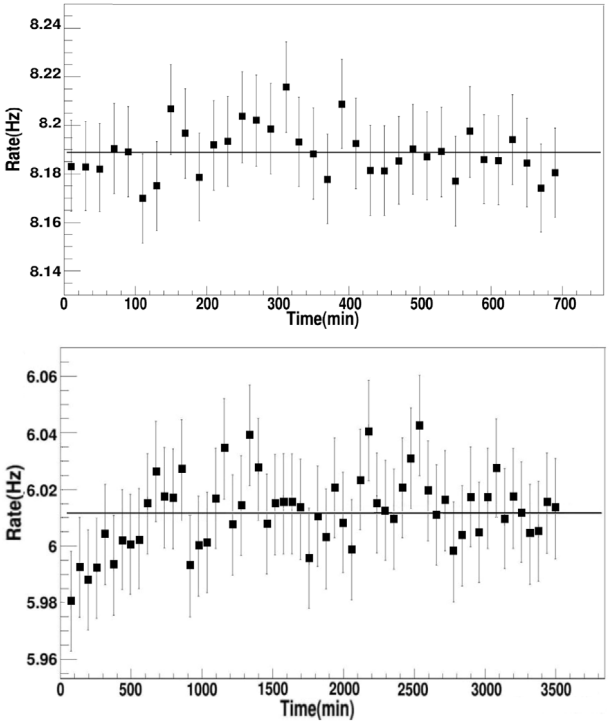

Fig. 18. LS coincidences as measured outdoor (top) and inside the Physics Department of Genova University (bottom).

operated by high school students. AstrO telescope is able to perform a variety of measurements: the integral intensity of cosmic muons, angular distribution, rate dependence on geographic location (latitude and altitude) and rate attenuation due to massive material such as concrete roof or rocks. Thanks to a solid design, it can measure with high statistics and systematic precision the integral rate with an excellent stability in time. A new version of the AstrO detector (AstrOPlano), currently under construction, will keep the main features of the current detector while providing an even more user friendly interface.

CRediT authorship contribution statement

S. Grazzi: Investigation, Data curation, Writing - original draft. **L. Assandri:** Investigation, Data curation. **M. Battaglieri:** Conceptualization, Project administration, Writing - review & editing. **C. Cardile:** Data curation, Investigation. **M. Corosu:** Software. **F. Fontanelli:** Software, Writing - review & editing. **G. Ottonello:** Resources. **F. Parodi:** Resources. **L. Perasso:** Software, Writing - review & editing. **F. Pratolongo:** Resources.

Declaration of competing interest

The authors declare that they have no known competing financial interests or personal relationships that could have appeared to influence the work reported in this paper.

Acknowledgments

This work was supported in part by Università di Genova, Italy and the Museo Storico della Fisica e Centro Studi e Ricerche Enrico Fermi, Italy. M.B. is supported by the U.S. Department of Energy, Office of Science, United States of America, Office of Nuclear Physics, United States of America under contract DE-AC05-06OR23177. A great thank goes to the Machine Workshop, the Computer Center and the Electronics Workshop of INFN Genova whose support was essential for the success of this project. We want also to thank students (in particular S. Bertolini, M. Pirovano and R. Vadalà) and Professors (in particular L. Battistella and C. Chiusa) of Liceo G. Casiraghi of Cinisello Balsamo, Milano — Italy that helped in calibrating, commissioning and testing the detector.

References

[1] S.E. Forbush, On the effects in cosmic-ray intensity observed during the recent magnetic storm, Phys. Rev. 51 (12) (1937) 108, http://dx.doi.org/10.1103/PhysRev.51.1108.3.
[2] L. Assandri, Progettazione e sviluppo di un telescopio portatile per muoni e neutroni cosmici (Master's thesis), Università di Genova, 2014-2015, (in italian).
[3] C. Cardile, Sviluppo di un sistema di controllo per un rivelatore di raggi cosmici basato su FPGA (Master's thesis), Università di Genova, 2016-2017, (in italian).
[4] Project extreme energy events - science inside schools (EEE) site, https://eee.centrofermi.it/.
[5] S. Bertolini, AstrO: a cosmic box for EEE, Liceo Giulio Casiraghi, Cinisello Balsamo (MI), Tesina Alternanza Scuola-Lavoro, 2019.
[6] M. Pirovano, AstrO: a portable cosmic ray detector, Liceo Giulio Casiraghi, Cinisello Balsamo (MI), Tesina Alternanza Scuola-Lavoro, 2019.
[7] R. Vadalà, Le misure di AstrO, Liceo Giulio Casiraghi, Cinisello Balsamo (MI), Tesina Alternanza Scuola-Lavoro, 2019.
[8] D. Beznosko, A. Bross, A. Dyshkant, A. Pla-Dalmau, V. Rykalin, FNAL-NICADD Extruded scintillator, Tech. Rep., Fermi National Accelerator Laboratory (FNAL), 2005, publication: FERMILAB-PUB-05-344.
[9] The CLAS12 Collaboration, CLAS12 - forward tagger (FT) – technical design report, Tech. Rep., 2005.
[10] Datasheets of SiPM and power supply can be found on Hamamatsu's site under the name of Mppc (multi-pixel photon counter), https://www.hamamatsu.com.
[11] De1-soc board to be found among Soc platforms employing Cyclone V FPGAs, search for Soc platform, Cyclone V family of FPGAs, www.terasic.com.tw.
[12] Datasheet of BME280 sensor chip, https://www.bosch-sensortec.com.
[13] QT: cross-platform application development framework, https://www.qt.io.
[14] GEMC, GEant4 Monte-Carlo, https://gemc.jlab.org/gemc/html/.
[15] GEANT4, a simulation toolkit, https://geant4.web.cern.ch/.
[16] M. Guan, M.C. Chu, J. Cao, K.B. Luk, C. Yang, A parametrization of the cosmic-ray muon flux at sea-level, 2015, arXiv e-prints, arXiv:1509.06176.
[17] T. Gaisser, T. Stanev, Cosmic rays in review of particle physics, Phys. Lett. B 592 (2018) http://pdg.lbl.gov.
[18] H.M. Kluck, Measurement of the cosmic-induced neutron yield at the modane underground laboratory (Ph.D. thesis), KIT, Karlsruhe, 2013, http://dx.doi.org/10.1007/978-3-319-18527-9, http://nbn-resolving.org/urn:nbn:de:swb:90-398379.
[19] M. Tanabashi, et al., Review of particle physics, Phys. Rev. D98 (3) (2018) 030001, http://dx.doi.org/10.1103/PhysRevD.98.030001.
[20] OULU cosmic ray station - neutron monitor, https://cosmicrays.oulu.fi/.
[21] G.L. tre, M. Vallarta, On compton's latitude effect of cosmic radiation, Phys. Rev. 43 (2) (1933) 87, http://dx.doi.org/10.1103/PhysRev.47.434.